From nonreciprocal to charge-4e supercurrent in Ge-based Josephson devices with tunable harmonic content

Axel Leblanc,[1,*] Chotivut Tangchingchai,[1] Zahra Sadre Momtaz,[2] Elyjah Kiyooka,[1] Jean-Michel Hartmann,[3] Gonzalo Troncoso Fernandez-Bada,[3] Zoltán Scherübl,[1,4,5] Boris Brun,[1] Vivien Schmitt,[1] Simon Zihlmann,[1] Romain Maurand,[1] Étienne Dumur,[1] Silvano De Franceschi,[1] and François Lefloch[1,†]

[1]*Université Grenoble Alpes, CEA, Grenoble INP, IRIG, PHELIQS, 38000 Grenoble, France*

[2]*Institut Néel, CNRS/UGA, Grenoble 38042, France*

[3]*Université Grenoble Alpes, CEA, LETI, 38000 Grenoble, France*

[4]*Department of Physics, Institute of Physics, Budapest University of Technology and Economics, H-1111 Budapest, Hungary*

[5]*MTA-BME Superconducting Nanoelectronics Momentum Research Group, H-111 Budapest, Hungary*

(Received 7 December 2023; accepted 12 July 2024; published 11 September 2024)

Hybrid superconductor(S)-semiconductor(Sm) devices bring a range of functionalities into superconducting circuits. In particular, hybrid parity-protected qubits and Josephson diodes were recently proposed and experimentally demonstrated. Such devices leverage the nonsinusoidal character of the Josephson current-phase relation (CPR) in highly transparent S-Sm-S junctions. Here, we report an experimental study of superconducting quantum-interference devices (SQUIDs) embedding Josephson field-effect transistors fabricated from a SiGe/Ge/SiGe heterostructure grown on a 200-mm silicon wafer. The single-junction CPR shows up to three harmonics with gate-tunable amplitude. In the presence of microwave irradiation, the ratio of the first two dominant harmonics, corresponding to single and double Cooper-pair transport processes, is consistently reflected in relative weight of integer and half-integer Shapiro steps. A combination of magnetic-flux and gate-voltage control enables tuning the SQUID functionality from a nonreciprocal Josephson-diode regime with 27% asymmetry to a π-periodic Josephson regime suitable for the implementation of parity-protected superconducting qubits. These results illustrate the potential of Ge-based hybrid devices as versatile and scalable building blocks of superconducting quantum circuits.

DOI: 10.1103/PhysRevResearch.6.033281

I. INTRODUCTION

The recent years have seen a revival of interest toward superconductor(S)-semiconductor(Sm) devices. These hybrid systems leverage, on the one hand, the macroscopic quantum coherence coming from superconductivity and, on the other hand, the field-effect charge control enabled by semiconductor materials. A typical example is the Josephson field-effect transistor (JoFET), a three-terminal device consisting of two superconducting contacts connected by a gate-tunable semiconducting channel. Owing to the superconducting proximity effect, a dissipationless supercurrent can flow through the normal-type semiconductor channel, with a maximal value, the so-called critical current, that depends on the applied gate voltage. A variety of JoFETs have been realized using different semiconductor materials. Some of these JoFETs were used to realize gate-tunable superconducting qubits often called gatemons [1–5] and parametric amplifiers [6–13].

In a JoFET, high-transparency S-Sm contacts enable the phase coherent transfer of m Cooper pairs at a time, resulting in the emergence of $\sin(m\varphi)$ components in the current phase relation (CPR) where φ is the phase difference between the two superconductors [14]. The gate permits to fine tune the critical current amplitude as well as the CPR harmonic composition [15].

In the context of superconducting qubits, the ability to tailor the CPR provides a means to engineer the support of the wave functions encoding the qubit. This idea has led to parity-protected qubits leveraging supercurrents carried by correlated pairs of Cooper pairs in $\sin(2\varphi)$ Josephson elements [16–19]. Along the same line, $\sin(2\varphi)$ Josephson elements for parity protection were recently obtained using S-Sm-S junctions with either an InAs [20,21] or, as in this work, a Ge channel [22]

Here, we investigate the CPR of a Ge-based Josephson junction using an asymmetric superconducting quantum-interference device (SQUID) featuring a wide and a narrow JoFET [23]. The CPR Fourier transform exhibits gate-tunable higher harmonics, revealing charge-2e, charge-4e, and charge-6e dissipationless transport. Notably, we observe the possibility of suppressing the higher harmonics by polarizing the JoFET near pinch-off. Subsequently, by investigating the response to microwave excitation, we observe half-integer Shapiro steps corroborating the existence of charge-4e supercurrents.

*Contact author: axel.leblanc@cea.fr

†Contact author: francois.lefloch@cea.fr

It was recently proposed [24,25] that nonsinusoidal CPR in nearly symmetric SQUIDs can lead to asymmetric transport characteristics. This behavior, commonly known as superconducting diode effect (SDE), requires time-reversal symmetry broken by a magnetic flux and is highly tunable, unlike previously reported realizations based on inversion symmetry breaking [26–30] or spin-orbit interaction in the presence of a magnetic field [31–37]. The diode efficiency vanishes when the SQUID operates in a perfectly symmetric regime, i.e., when the two junctions have the same CPR, or when the SQUID is flux-biased at half the flux quantum. By harnessing the SDE within a SQUID made of two similar JoFETs (we observe diode efficiency up to 27%), we identify its regime of critical current balance. In this configuration, Shapiro step measurements at half-flux quantum bias evidence a pronounced reduction in the odd harmonics due to destructive interference within the SQUID.

This realization yields a device primarily governed by a charge-4e supercurrent, effectively creating a $\sin(2\varphi)$ Josephson element, thus opening the way to the development of Ge-based parity-protected qubits.

II. DEVICE AND MATERIAL PROPERTIES

The initial heterostructure consists of a 2.5-μm-thick $Si_{0.21}Ge_{0.79}$ virtual substrate grown on a 200-mm Si(001) wafer. To reach this high Ge content, the Ge concentration is linearly increased from 0 up to 79% at a rate of 10%/μm. A strained 16-nm-thick Ge quantum well is grown on top of the polished virtual substrate and covered by a 22-nm-thick $Si_{0.21}Ge_{0.79}$ layer and a 2-nm-thick Si cap layer. In the accumulation regime the hole mobility μ_h measured in $60 \times 600\,\mu m^2$ Hall bars reaches $1 \times 10^5\,cm^2\,V^{-1}\,s^{-1}$ and a corresponding elastic mean free path of $l_e \approx 1.5\,\mu m$ [38].

The fabrication of the Ge JoFETs starts with the etching of a long mesa (typically 5 μm) with various widths ranging from 1 μm to 10 μm. In a second step, the superconducting contacts are defined by locally etching the Si cap layer and the SiGe top layer, followed by the *ex situ* deposition and lift-off of a 50-nm-thick Al layer in contact with the Ge quantum well. The aluminium contact has a typical critical temperature of 1.54 K. Both etching steps are done using a dry reactive ion etching process with fluoride and argon-based plasma. An AlO_x oxide is then deposited everywhere using atomic layer deposition (ALD). To finish the process, a Ti/Au top gate covers the Ge central channel and slightly overlaps the Al contacts [Fig. 1(a)]. See Supplemental Material S-I [59] for more details on the characterization of the devices.

The asymmetric SQUID consists of two Al-Ge-Al JoFETs placed in an Al loop [Fig. 1(b)]. The narrow junction J_n has a width of 1 μm, while the wide junction J_w is 8 μm wide. Both junctions are 300 nm long. In the following experiments, the devices are cooled down to a base temperature of 35 mK. To measure the electrical behavior of J_n (J_w) independently, we apply a large gate voltage on J_w (J_n) (typically +4 V) to suppress the conductance on the respective arm of the SQUID. Both junctions can be fully proximitized and show a nondissipative current up to a certain switching current (identified as the critical current) that is gate tunable. At full accumulation ($V_G = -2$V), the critical currents are $I_C^n = 158$ nA and

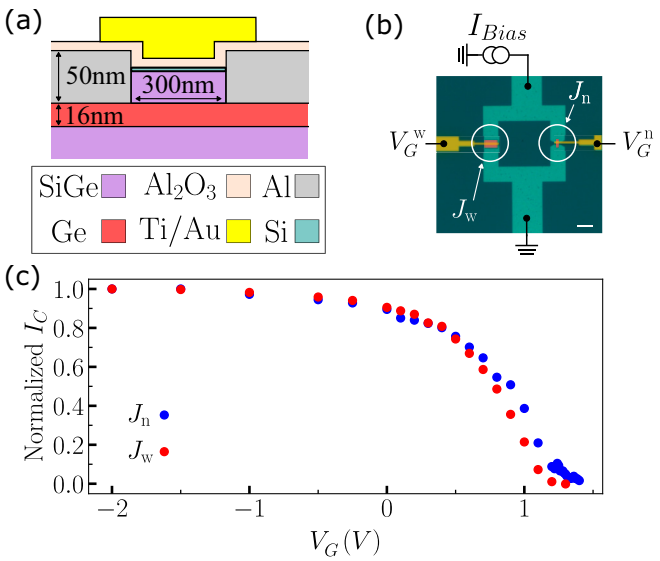

FIG. 1. JoFETs placed in a SQUID. (a) Cross-section sketch of a JoFET where the Ge quantum well is contacted by two superconducting aluminium leads. The Ti/Au top gate allows to modify the hole carrier density in the channel. (b) False color scanning electron microscopy (SEM) image of the SQUID with a wide (left) and a narrow (right) junction placed in an aluminium loop (green). Electrostatic gates are shown in yellow. The scale bar is 10 μm. (c) Critical current of the two junctions normalized to their values at $V_G = -2$ V.

$I_C^w = 2.39$ μA with very remarkable similar gate dependency [Fig. 1(c)]. The I_cR_N product of both junctions are of the order of 100 μeV and very close to the state of the art [39–43].

The symmetric SQUID device used to study the SDE is composed of two nearly identical junctions with $W = 4\,\mu m$ and $L = 300$ nm and shows similar tunable critical current at low temperature.

III. CURRENT-PHASE RELATION OF A SINGLE GE/Al JoFET

The loop dimensions of the asymmetric SQUID used for CPR measurements have been chosen large enough to avoid Fraunhofer reduction in the flux range of interest (see Supplemental Material S-III [59]). The width of the loop arms is 10 μm and the associated self-inductance is estimated to be 102 pH. Its contribution to the measurement is negligible and discussed in Supplemental Material S-II [59].

The total supercurrent I_{SQUID} flowing through the SQUID is the sum of the current flowing through each junction and thus includes the two current phase relations $I_w(\varphi_w)$ and $I_n(\varphi_n)$. Since one junction is much wider than the other, its critical current I_C^w is also much larger than that of the narrow junction I_C^n ($I_C^w/I_C^n = 15$). Thus, the maximum supercurrent through the SQUID is reached at $\varphi_w \approx \pi/2$ i.e. when the maximum current through J_w is reached. Taking into account the fluxoid relationship that relates the superconducting phases to the applied magnetic flux, the total critical current flux dependency of the SQUID can be written as

$$I_C^{SQUID} = I_w(\pi/2) + I_n(\pi/2 + 2\pi\,\Phi_{ext}/\Phi_0) \qquad (1)$$

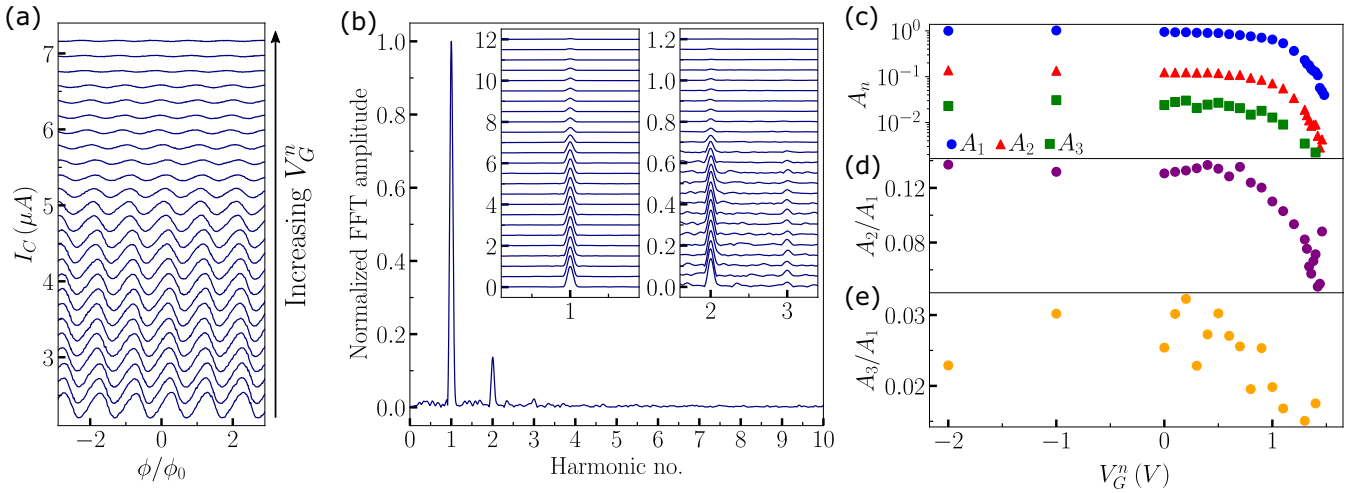

FIG. 2. Gate modulation of the CPR harmonic content. (a) I_c modulations (shifted for clarity) of the asymmetric SQUID as a function of the flux for various $V_G^{\rm n}$ [each line corresponds to one point in (c), (d), and (e)] from full accumulation ($V_G^{\rm n} = -2$ V) to near threshold ($V_G^{\rm n} = 1.48$ V) with a fixed gate voltage applied to the wide junction ($V_G^{\rm w} = -2$ V). (b) Fast Fourier transform (FFT) (normalized to the first harmonic amplitude) of $I_C(\phi)$ at $V_G^{\rm n} = -2$ V and, in the insets, for the same $V_G^{\rm n}$ range as in (a) (shifted for clarity). The three first harmonics are clearly visible and higher harmonics disappear faster when $V_G^{\rm n}$ gets close to the threshold voltage. (c) Amplitude of the first three harmonics A_1, A_2, and A_3 (in log scale) versus the gate voltage $V_G^{\rm n}$. All of them tend to decrease with gate voltage since the overall flux modulation of I_C decreases. (d) and (e) Ratio between the second and third, respectively, and the first harmonic amplitudes. The ratios decreasing highlights the disappearance of higher harmonics before the first one and thus a transition from a multi harmonics CPR toward a more sinusoidal one.

where $\Phi_{\rm ext}$ is the magnetic flux threading the loop and $\Phi_0 = h/2e$ the superconducting flux quantum.

One can clearly see that measuring the critical current of the whole SQUID $I_C^{\rm SQUID}$ versus the applied flux $\Phi_{\rm ext}$ allows to probe the current phase relation of the narrow junction $\rm J_n$ [23] (see Supplemental Material S-III [59] for details on the measurement protocol).

For this experiment, the wide junction $\rm J_w$ is kept in the full accumulation regime ($V_G^{\rm w} = -2$ V). As expected, oscillations of the SQUID critical current are observed, as well as a background curvature associated with the Fraunhofer effect on the wide junction (see Supplemental Material S-III [59]). The flux modulation $I_C(\Phi_{\rm ext})$, studied for different values of the gate voltage $V_G^{\rm n}$ and shown in Fig. 2(a) after numerically removing the background, is a direct measurement of the CPR of the narrow junction.

One can already notice that $I_C(\Phi_{\rm ext})$ is skewed in the highly accumulated regime, suggesting the presence of higher harmonics. In order to better evidence the skewness and to quantify the various components of the CPR, we applied a Fourier transform to these data over 25 periods [Fig. 2(b)].

The spectral decomposition at full accumulation ($V_G^{\rm n} = -2$ V) is shown in Fig. 2(b). The result shows a clear contribution from the first and second harmonics, and also from the third harmonic but with less pronounced evidence. This confirms that the CPR is not purely sinusoidal. The insets of Fig. 2(b) show the gate dependence of the three harmonics. The first harmonic survives up to the largest gate voltages applied ($V_G^{\rm n} = 1.48$ V), while the second and third harmonics vanish at a lower gate voltage.

The amplitude of the three first harmonics are extracted by taking the height of each peak in the Fourier decomposition. A_n is the weight of the nth harmonic and is plotted as a function of V_G^n in Fig. 2(c). When $V_G^{\rm n}$ approaches the threshold voltage ($V_{th} \approx 1.5$ V), we observe a reduction of all harmonic amplitudes consistent with the reduction of the critical current. The ratio between A_2 (A_3) and A_1 shown in Fig. 2(d) [Fig. 2(e)] goes up to 0.13 (0.03). Interestingly, the gate dependence reveals the faster disappearance of higher harmonics compared to the main one. As mentioned above, higher harmonics in the CPR are intrinsic to the proximitized Josephson junctions. We have checked (see Supplemental Material S-V [59]) that multiple harmonics cannot originate from arm inductances as is the case with S-I-S junctions. The faster disappearance of the higher harmonics reveals a change in the CPR as the proximitized Ge region gets depleted from carriers.

The overall decrease of the nondissipative current is consistent with the reduction of the number of conducting channels and of their mean transparency when the gate voltage approaches the threshold (see Supplemental Material S-I [59]). Together, the Fermi velocity decreases and so is the proximity effect (through the reduction of penetration of Andreev pairs in the Ge channel). All these effects contribute to modify the harmonic's content of the CPR as a function of the gate voltage [14,44].

IV. SHAPIRO STEPS IN A SINGLE GE/AL JoFET

In the previous section, we have shown the results of the direct measurement of the CPR of the narrow junction. Thanks to the high gate control of our Ge-based JoFET, the wide junction of the exact same SQUID device can be tuned in the very depleted regime at $V_G^{\rm w} = 4$ V where the conductance is zero. The device is now only composed of the narrow junction for which the CPR is known.

In the following, we focus on the ac Josephson effect of the narrow junction, which should highlight the presence of higher harmonics in the CPR. Under microwave irradiation

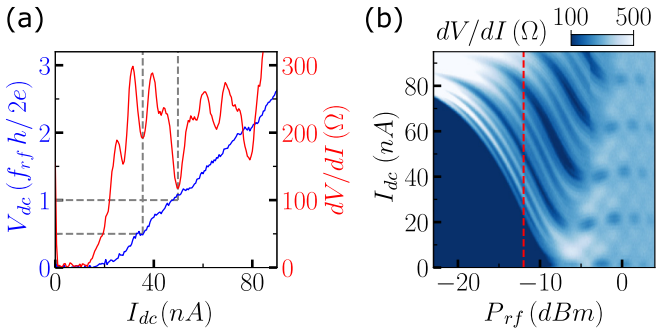

FIG. 3. Integer and half-integer Shapiro steps. (a) dc voltage normalized to the expected Shapiro step positions (blue line) and differential resistance (red line) as function of the bias current $I_{\rm dc}$ under radio-frequency irradiation at $f = 3.05$ GHz with a power $P_{\rm rf} = -12$ dBm [see the dashed red line in (b)]. The dashed gray lines are guides to the eye for the first half-integer and integer steps. (b) Differential resistance as a function of the bias current $I_{\rm dc}$ as well as the microwave power $P_{\rm rf}$. Integer (wide dark lines) and half-integer (narrow dark lines) follow the Bessel like oscillations as a function of the rf power.

at frequency f, the current-voltage characteristic shows steps at some specific voltages $V = nhf/2e$, where h is the Plank constant, e the elementary charge, and $n = 0, 1, 2, \ldots$ are called Shapiro steps [45]. If the CPR of the Josephson junction contains a second harmonic, half-integer Shapiro steps also appear ($n = 1/2, 3/2, \ldots$) indicating the coherent transport of pairs of Cooper pairs through the junction (i.e., a charge-4e supercurrent) [46,47].

Figure 3(a) shows the differential resistance measurement (red line) and the measured dc voltage (blue line) as a function of the current bias under a radio-frequency irradiation at $f = 3.05$ GHz and with a fixed microwave power $P_{\rm rf} = -12$ dBm. We identify clear dips in the differential resistance that correspond to integer and half-integer Shapiro steps (highlighted by dashed gray lines).

Figure 3(b) shows the differential resistance as a function of the microwave drive power $P_{\rm rf}$ and the dc bias $I_{\rm dc}$. Dark regions correspond to dips in the differential resistance and are associated with Shapiro steps. The widths of these steps follow the usual Bessel-like behavior [48]. The clear observation of half-integer steps is perfectly consistent with previously measured harmonic content of the CPR.

By applying more positive gate voltages ($V_G^{\rm n}$ near threshold), one would expect half-integer steps to disappear before integer ones as the CPR becomes purely sinusoidal. The quantitative analysis of this effect is challenging because of the overlap of the different step signals for such rounded steps. Shapiro patterns for different gate voltages are shown in Supplemental Material S-IV [59].

As an intermediate conclusion, we have shown that proximitized planar SiGe-based Josephson junctions exhibit intrinsic non purely sinusoidal current phase relation. This response has been probed and measured in a single junction, first in a SQUID geometry to directly measure the CPR and under radio-frequency irradiation to reveal half-integer Shapiro steps. This has been made possible thanks to the high gate tunability of the SiGe JoFETs.

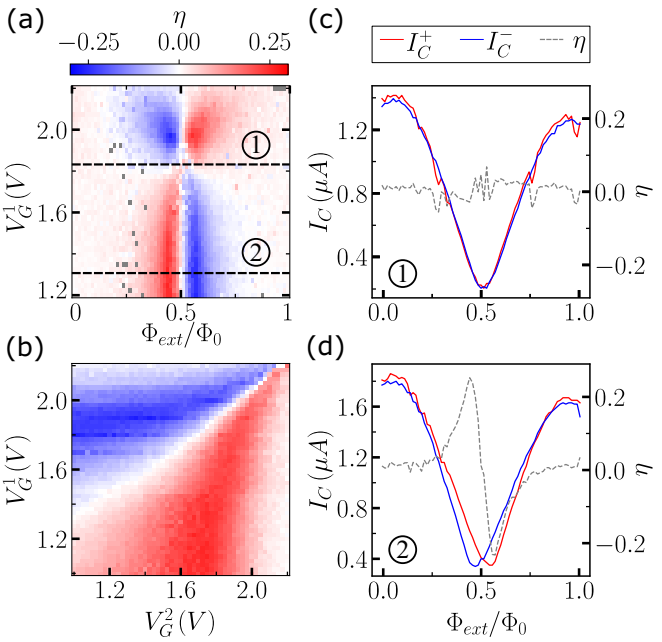

FIG. 4. Gate and flux dependence of the superconducting diode effect. (a) Diode efficiency η as function of the normalized applied flux $\Phi_{\rm ext}/\Phi_0$ and V_G^1 for a fixed $V_G^2 = 1.75$ V. η vanishes at half-flux quantum $\Phi_{\rm ext}/\Phi_0 = 0.5$ and for the peculiar gate voltage $V_G^1 = 1.825$ V. (b) Diode efficiency as a function of the two gate voltages V_G^1 and V_G^2 for a fixed flux biasing slightly below the half-flux quantum $\Phi_{\rm ext}/\Phi_0 = 0.45$. The white line corresponds to perfectly symmetric regime where the SDE disappears. (c) and (d) Forward I_c^+ (red line) and backward I_c^- (blue line) critical currents and extracted diode efficiency η as a function of the normalized applied flux $\Phi_{\rm ext}/\Phi_0$ for $V_G^1 = 1.75$ V and $V_G^1 = 1.3$ V.

V. SUPERCONDUCTING DIODE EFFECT IN A SYMMETRIC SQUID

In a SQUID with negligible arms inductances, SDE can still emerge if at least one of the junctions has a nonsinusoidal CPR [22,24,49,50]. To investigate this possibility, we have fabricated a SQUID with two nominally identical JoFETs, J_1 and J_2 with W = 4 μm and L = 300 nm. The diode effect arises if (1) the external flux is not an integer multiple of the half-flux quantum $\Phi = n\Phi_0/2$ and (2) the two CPRs of the two junctions are not perfectly balanced. The SDE can be quantified through the diode efficiency

$$\eta = \frac{I_C^+ - I_C^-}{I_C^+ + I_C^-}, \tag{2}$$

where I_C^+ and I_C^- are the forward and backward critical currents of the SQUID.

Figure 4(a) shows the diode efficiency η as a function of the gate voltage of J_1 (V_G^1) and the normalized flux $\Phi_{\rm ext}/\Phi_0$ for a fixed value of $V_G^2 = 1.75$ V together with two $I_c^{+(-)}$ traces [Figs. 4(c) and 4(d)] from which the efficiency is calculated. As expected, the diode efficiency vanishes at half the flux quantum and follows very well the predicted behavior [24] with a maximum that goes up to 27%. At $V_G^1 = 1.825$ V [Fig. 4(c)] the diode efficiency drops to zero for any flux value. This suggests that for this combination of gate voltages the

SQUID is perfectly symmetric. But this gate values combination is not unique.

To find every gate configuration that perfectly balances the SQUID, the device is flux-biased slightly below the half-flux quantum ($\Phi_{ext} = 0.45\Phi_0$) and the diode efficiency measured as a function of V_G^1 and V_G^2. The result [Fig. 4(b)] highlights the existence of a line (in white) corresponding to all gate voltage combinations where the SQUID operates in a perfectly balanced regime. The critical current of the SQUID along this line is shown in Supplemental Material S-VI [59]. The fact that this line does not follow the $V_G^1 = V_G^2$ diagonal means that the two JoFETs have fairly close yet not identical characteristics. Nevertheless, the symmetric situation can be easily obtained thanks to the independent tunability of the junctions.

VI. SHAPIRO STEPS IN A PERFECTLY SYMMETRIC SQUID

In the previous section we have shown that the SDE observed in a symmetric SQUID is consistent with the non-sinusoidal CPR of the junctions. We have also demonstrated that the contribution of the various harmonics strongly depends on the applied magnetic flux threading the SQUID. Moreover, as detailed before, dc Shapiro steps observed under radio-frequency irradiation can also reveal CPR multiple harmonics. In this section, we present the results of Shapiro steps measured in the exact same SQUID as the one used to reveal SDE. To do so, we operate the SQUID for a fixed set of gate voltages $V_G^1 = 1.825$ V and $V_G^2 = 1.75$ V, which correspond to one of the symmetric regime combinations, and vary the magnetic flux.

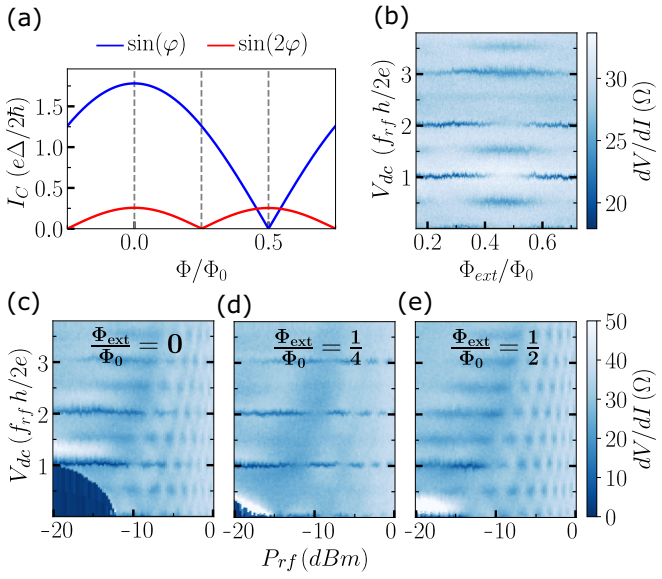

FIG. 5. Half-integer Shapiro steps as a probe for $\sin(2\varphi)$ CPR. (a) Computation of the first two harmonics amplitudes of a symmetric SQUID CPR for a single-channel short junction model with a transparency $\tau = 0.7$ (see Supplemental Material S-IX [59]). (b) Differential resistance as a function of the normalized dc voltage and the applied flux normalized to ϕ_0 for a fixed $P_{rf} = -8$ dBm and in the balanced regime ($V_G^1 = 1.825$ V and $V_G^2 = 1.75$ V). Dark lines correspond to differential resistance dips associated to Shapiro steps. (b), (d), and (e) Differential resistance as a function of the normalized dc voltage and the rf excitation power at fixed applied flux $\Phi_{ext} = 0$, $\Phi_0/4$, and $\Phi_0/2$ respectively.

Figure 5(a) is the theoretical amplitudes of the first and second harmonics as a function of the flux threading in a symmetric SQUID (see Supplemental Material S-IX [59]). Figure 5(b) shows the differential resistance of the SQUID as a function of the applied external flux Φ_{ext} and the dc voltage V_{dc} normalized to the expected Shapiro steps positions, for a given microwave radiation power $P_{rf} = -8$ dBm and frequency $f = 7$ GHz. Dark blue ridges reveal the position of the Shapiro steps and evidence the emergence of half-integer steps around $\Phi_0/2$. Figures 5(c)–5(e) show the differential resistance as a function of the microwave radiation power and the normalized dc voltage for three different fluxes $\Phi_{ext} = 0$, $\Phi_{ext} = \Phi_0/2$, and $\Phi_{ext} = \Phi_0/4$ corresponding to the dashed gray lines in Fig. 5(a). At $\Phi_{ext} = \Phi_0$, both integer and half-integer steps are visible with a stronger intensity of the integer steps and follow the Bessel-type oscillations as a function of the power. At $\Phi_{ext} = \Phi_0/2$ integer and half-integer steps are still visible but with a relative contrast that is weaker than for $\Phi_{ext} = 0$. This reduction is consistent with the vanishing of the first harmonic at $\Phi_{ext} = \Phi_0/2$ but where integer steps correspond to a multiple-photons process of half-integer steps. At $\Phi_{ext} = \Phi_0/4$, however, the contribution of the second CPR harmonic vanishes and the half-integer steps disappear completely. Therefore, we demonstrated the flux-tunability of the first and second harmonics, opening the possibility to engineer a $\sin(2\varphi)$ Josephson element dominated by charge-4e supercurrent.

VII. CONCLUSION

In conclusion, our work harnesses the high gate tunability offered by SiGe-based proximitized Josephson junctions to conduct comprehensive measurements of the CPR and Shapiro steps within a single JoFET. The CPR clearly reveals gate-tunable non purely sinusoidal phase dependence, reveling higher-order harmonics that correspond to the coherent transfer of both single and multiple Cooper pairs. This observation is supported by the presence of both integer and half-integer Shapiro steps. We also revealed a gate and flux-tunable SDE in a SQUID geometry, made possible once again by the JoFETs high transparency and gate tunability [24]. Ultimately, we demonstrated the realization of a so-called $\sin(2\varphi)$ Josephson element in a SQUID biased at half-flux quantum and finely gate-tuned to its balanced critical current point. Our results underscore the remarkable potential of the SiGe-based heterostructures for the realization of parity-protected superconducting qubits without the need for large inductance engineering as required with tunnel S-I-S junctions [18,20,51]. Our study focused on wide junctions, ranging from 1 to 10 μm, with critical current spanning from a few hundred nA to a few μA. These values suggest that narrower junctions, probably necessary to avoid Andreev bound states at low energies, will still have a large enough Josephson energy for the realization of suitable gatemon qubits. Moreover, such materials are fully compatible with the Com-

plementary Metal-Oxide-Semiconductor (CMOS) technology and potentially large-scale integration.

ACKNOWLEDGMENTS

This work has been supported by the ANR project SUNISIDEuP (Grant No. ANR-19-CE47-0010), the PEPR ROBUSTSUPERQ (Grant No. ANR-22-PETQ-0003), PEPR PRESQUILE (Grant No. ANR-22-PETQ-0002), the ERC starting Grant LONGSPIN (Grant No. Horizon 2020-759388), the ERC Grant e-See (Grant No. Horizon 2020 - 758385), and the Grenoble LaBEX LANEF. We thank Frederic Gustavo and Jean-Luc Thomassin for their contribution in the nanofabrication at the PTA (CEA-Grenoble) and the CNRS Neel Institute for access to the Nanofab facility.

[1] T. W. Larsen, K. D. Petersson, F. Kuemmeth, T. S. Jespersen, P. Krogstrup, J. Nygård, and C. M. Marcus, Semiconductor-nanowire-based superconducting qubit, Phys. Rev. Lett. **115**, 127001 (2015).

[2] G. de Lange, B. van Heck, A. Bruno, D. J. van Woerkom, A. Geresdi, S. R. Plissard, E. P. A. M. Bakkers, A. R. Akhmerov, and L. DiCarlo, Realization of microwave quantum circuits using hybrid superconducting-semiconducting nanowire Josephson elements, Phys. Rev. Lett. **115**, 127002 (2015).

[3] L. Casparis, T. W. Larsen, M. S. Olsen, F. Kuemmeth, P. Krogstrup, J. Nygård, K. D. Petersson, and C. M. Marcus, Gatemon benchmarking and two-qubit operations, Phys. Rev. Lett. **116**, 150505 (2016).

[4] L. Casparis, M. R. Connolly, M. Kjaergaard, N. J. Pearson, A. Kringhøj, T. W. Larsen, F. Kuemmeth, T. Wang, C. Thomas, S. Gronin, G. C. Gardner, M. J. Manfra, C. M. Marcus, and K. D. Petersson, Superconducting gatemon qubit based on a proximitized two-dimensional electron gas, Nat. Nanotechnol. **13**, 915 (2018).

[5] J. I.-J. Wang, D. Rodan-Legrain, L. Bretheau, D. L. Campbell, B. Kannan, D. Kim, M. Kjaergaard, P. Krantz, G. O. Samach, F. Yan, J. L. Yoder, K. Watanabe, T. Taniguchi, T. P. Orlando, S. Gustavsson, P. Jarillo-Herrero, and W. D. Oliver, Coherent control of a hybrid superconducting circuit made with graphene-based van der Waals heterostructures, Nat. Nanotechnol. **14**, 120 (2019).

[6] G. Butseraen, A. Ranadive, N. Aparicio, K. R. Amin, A. Juyal, M. Esposito, K. Watanabe, T. Taniguchi, N. Roch, F. Lefloch, and J. Renard, A gate-tunable graphene Josephson parametric amplifier, Nat. Nanotechnol. **17**, 1153 (2022).

[7] J. Sarkar, K. V. Salunkhe, S. Mandal, S. Ghatak, A. H. Marchawala, I. Das, K. Watanabe, T. Taniguchi, R. Vijay, and M. M. Deshmukh, Quantum noise limited microwave amplification using a graphene Josephson junction, Nat. Nanotechnol. **17**, 1147 (2022).

[8] D. Phan, P. Falthansl-Scheinecker, U. Mishra, W. Strickland, D. Langone, J. Shabani, and A. Higginbotham, Gate-tunable superconductor-semiconductor parametric amplifier, Phys. Rev. Appl. **19**, 064032 (2023).

[9] L. J. Splitthoff, J. J. Wesdorp, M. Pita-Vidal, A. P. Bargerbos, and C. K. Andersen, Gate-tunable kinetic inductance parametric amplifier, Phys. Rev. Appl. **21**, 014052 (2024).

[10] W. M.Strickland, L. J. Baker, J. Lee, K. Dindial, B. H. Elfeky, P. J. Strohbeen, M. Hatefipour, P. Yu, I. Levy, J. Issokson, V. E. Manucharyan, and J. Shabani, Characterizing losses in InAs two-dimensional electron gas-based gatemon qubits, Phys. Rev. Res. **6**, 023094 (2024).

[11] J. Huo, Z. Xia, Z. Li, S. Zhang, Y. Wang, D. Pan, Q. Liu, Y. Liu, Z. Wang, Y. Gao, J. Zhao, T. Li, J. Ying, R. Shang, and H. Zhang, Gatemon qubit based on a thin InAs-Al hybrid nanowire, Chin. Phys. Lett. **40**, 047302 (2023).

[12] A. Hertel, M. Eichinger, L. O. Andersen, D. M. van Zanten, S. Kallatt, P. Scarlino, A. Kringhøj, J. M. Chavez-Garcia, G. C. Gardner, S. Gronin, M. J. Manfra, A. Gyenis, M. Kjaergaard, C. M. Marcus, and K. D. Petersson, Gate-tunable transmon using selective-area-grown superconductor-semiconductor hybrid structures on silicon, Phys. Rev. Appl. **18**, 034042 (2022).

[13] E. Zhuo, Z. Lyu, X. Sun, A. Li, B. Li, Z. Ji, J. Fan, E. P. a. M. Bakkers, X. Han, X. Song, F. Qu, G. Liu, J. Shen, and L. Lu, Hole-type superconducting gatemon qubit based on Ge/Si core/shell nanowires, npj Quantum Inf. **9**, 51 (2023).

[14] W. Haberkorn, H. Knauer, and J. Richter, A theoretical study of the current-phase relation in Josephson contacts, Physica Stat. Sol. (a) **47**, K161 (1978).

[15] E. M. Spanton, M. Deng, S. Vaitiekėnas, P. Krogstrup, J. Nygård, C. M. Marcus, and K. A. Moler, Current–phase relations of few-mode InAs nanowire Josephson junctions, Nat. Phys. **13**, 1177 (2017).

[16] S. Gladchenko, D. Olaya, E. Dupont-Ferrier, B. Douçot, L. B. Ioffe, and M. E. Gershenson, Superconducting nanocircuits for topologically protected qubits, Nat. Phys. **5**, 48 (2009).

[17] B. Douçot and L. B. Ioffe, Physical implementation of protected qubits, Rep. Prog. Phys. **75**, 072001 (2012).

[18] W. C. Smith, A. Kou, X. Xiao, U. Vool, and M. H. Devoret, Superconducting circuit protected by two-Cooper-pair tunneling, npj Quantum Inf. **6**, 8 (2020).

[19] W. C. Smith, M. Villiers, A. Marquet, J. Palomo, M. R. Delbecq, T. Kontos, P. Campagne-Ibarcq, B. Douçot, and Z. Leghtas, Magnifying quantum phase fluctuations with Cooper-pair pairing, Phys. Rev. X **12**, 021002 (2022).

[20] T. W. Larsen, M. E. Gershenson, L. Casparis, A. Kringhøj, N. J. Pearson, R. P. G. McNeil, F. Kuemmeth, P. Krogstrup, K. D. Petersson, and C. M. Marcus, Parity-protected superconductor-semiconductor qubit, Phys. Rev. Lett. **125**, 056801 (2020).

[21] C. Ciaccia, R. Haller, A. C. C. Drachmann, T. Lindemann, M. J. Manfra, C. Schrade, and C. Schönenberger, Charge-4e supercurrent in an InAs-Al superconductor-semiconductor heterostructure, Commun. Phys. **7**, 41 (2024).

[22] M. Valentini, O. Sagi, L. Baghumyan, T. de Gijsel, J. Jung, S. Calcaterra, A. Ballabio, J. A. Servin, K. Aggarwal, M. Janik, T. Adletzberger, R. S. Souto, M. Leijnse, J. Danon, C. Schrade, E. Bakkers, D. Chrastina, G. Isella, and G. Katsaros, Parity-

conserving Cooper-pair transport and ideal superconducting diode in planar Germanium, Nat. Commun. **15**, 169 (2024).

[23] M. L. Della Rocca, M. Chauvin, B. Huard, H. Pothier, D. Esteve, and C. Urbina, Measurement of the current-phase relation of superconducting atomic contacts, Phys. Rev. Lett. **99**, 127005 (2007).

[24] R. S. Souto, M. Leijnse, and C. Schrade, Josephson diode effect in supercurrent interferometers, Phys. Rev. Lett. **129**, 267702 (2022).

[25] Ya. V. Fominov and D.S. Miklailov, Asymmetric higher-harmonic SQUID as a Josephson diode, Phys. Rev. B **106**, 134514 (2022).

[26] F. Ando, Y. Miyasaka, T. Li, J. Ishizuka, T. Arakawa, Y. Shiota, T. Moriyama, Y. Yanase, and T. Ono, Observation of superconducting diode effect, Nature (London) **584**, 373 (2020).

[27] L. Bauriedl, C. Bäuml, L. Fuchs, C. Baumgartner, N. Paulik, J. M. Bauer, K.-Q. Lin, J. M. Lupton, T. Taniguchi, K. Watanabe, C. Strunk, and N. Paradiso, Supercurrent diode effect and magnetochiral anisotropy in few-layer $NbSe_2$, Nat. Commun. **13**, 4266 (2022).

[28] A. Daido, Y. Ikeda, and Y. Yanase, Intrinsic superconducting diode effect, Phys. Rev. Lett. **128**, 037001 (2022).

[29] S. Matsuo, T. Imoto, T. Yokoyama, Y. Sato, T. Lindemann, S. Gronin, G. C. Gardner, M. J. Manfra, and S. Tarucha, Josephson diode effect derived from short-range coherent coupling, Nat. Phys. **19**, 1636 (2023).

[30] J.-D. Pillet, S. Annabi, A. Peugeot, H. Riechert, E. Arrighi, J. Griesmar, and L. Bretheau, Josephson diode effect in Andreev molecules, Phys. Rev. Res. **5**, 033199 (2023).

[31] T. Yokoyama, M. Eto, and Y. V. Nazarov, Anomalous Josephson effect induced by spin-orbit interaction and Zeeman effect in semiconductor nanowires, Phys. Rev. B **89**, 195407 (2014).

[32] A. Zazunov, R. Egger, T. Jonckheere, and T. Martin, Anomalous Josephson current through a spin-orbit coupled quantum dot, Phys. Rev. Lett. **103**, 147004 (2009).

[33] K. Halterman, M. Alidoust, R. Smith, and S. Starr, Supercurrent diode effect, spin torques, and robust zero-energy peak in planar half-metallic trilayers, Phys. Rev. B **105**, 104508 (2022).

[34] E. Strambini, M. Spies, N. Ligato, S. Ilić, M. Rouco, C. González-Orellana, M. Ilyn, C. Rogero, F. S. Bergeret, J. S. Moodera, P. Virtanen, T. T. Heikkilä, and F. Giazotto, Superconducting spintronic tunnel diode, Nat. Commun. **13**, 2431 (2022).

[35] G. P. Mazur, N. van Loo, D. van Driel, J.-Y. Wang, G. Badawy, S. Gazibegovic, E. P. A. M. Bakkers, and L. P. Kouwenhoven, The gate-tunable Josephson diode, arXiv:2211.14283.

[36] C. Baumgartner, L. Fuchs, A. Costa, S. Reinhardt, S. Gronin, G. C. Gardner, T. Lindemann, M. J. Manfra, P. E. Faria Junior, D. Kochan, J. Fabian, N. Paradiso, and C. Strunk, Supercurrent rectification and magnetochiral effects in symmetric Josephson junctions, Nat. Nanotechnol. **17**, 39 (2022).

[37] B. Turini, S. Salimian, M. Carrega, A. Iorio, E. Strambini, F. Giazotto, V. Zannier, L. Sorba, and S. Heun, Josephson diode effect in high-mobility InSb nanoflags, Nano Lett. **22**, 8502 (2022).

[38] J.-M. Hartmann, N. Bernier, F. Pierre, J.-P. Barnes, V. Mazzocchi, J. Krawczyk, G. Lima, E. Kiyooka, and S. D. Franceschi, Epitaxy of group-IV semiconductors for quantum electronics, ECS Transactions **111**, 53 (2023).

[39] N. W. Hendrickx, M. L. V. Tagliaferri, M. Kouwenhoven, R. Li, D. P. Franke, A. Sammak, A. Brinkman, G. Scappucci, and M. Veldhorst, Ballistic supercurrent discretization and micrometer-long Josephson coupling in germanium, Phys. Rev. B **99**, 075435 (2019).

[40] F. Vigneau, R. Mizokuchi, D. C. Zanuz, X. Huang, S. Tan, R. Maurand, S. Frolov, A. Sammak, G. Scappucci, F. Lefloch, and S. De Franceschi, Germanium quantum-well Josephson field-effect transistors and interferometers, Nano Lett. **19**, 1023 (2019).

[41] K. Aggarwal, A. Hofmann, D. Jirovec, I. Prieto, A. Sammak, M. Botifoll, S. Martí-Sánchez, M. Veldhorst, J. Arbiol, G. Scappucci, J. Danon, and G. Katsaros, Enhancement of proximity-induced superconductivity in a planar Ge hole gas, Phys. Rev. Res. **3**, L022005 (2021).

[42] A. Tosato, V. Levajac, J.-Y. Wang, C. J. Boor, F. Borsoi, M. Botifoll, C. N. Borja, S. Martí-Sánchez, J. Arbiol, A. Sammak, M. Veldhorst, and G. Scappucci, Hard superconducting gap in germanium, Commun. Mater. **4**, 23 (2023).

[43] J. Xiang, A. Vidan, M. Tinkham, R. M. Westervelt, and C. M. Lieber, Ge/Si nanowire mesoscopic Josephson junctions, Nat. Nanotechnol. **1**, 208 (2006).

[44] A. A. Golubov, M. Y. Kupriyanov, and E. Il'ichev, The current-phase relation in Josephson junctions, Rev. Mod. Phys. **76**, 411 (2004).

[45] S. Shapiro, Josephson currents in superconducting tunneling: The effect of microwaves and other observations, Phys. Rev. Lett. **11**, 80 (1963).

[46] K. Ueda, S. Matsuo, H. Kamata, Y. Sato, Y. Takeshige, K. Li, L. Samuelson, H. Xu, and S. Tarucha, Evidence of half-integer Shapiro steps originated from nonsinusoidal current phase relation in a short ballistic InAs nanowire Josephson junction, Phys. Rev. Res. **2**, 033435 (2020).

[47] A. Iorio, A. Crippa, B. Turini, S. Salimian, M. Carrega, L. Chirolli, V. Zannier, L. Sorba, E. Strambini, F. Giazotto, and S. Heun, Half-integer Shapiro steps in highly transmissive InSb nanoflag Josephson junctions, Phys. Rev. Res. **5**, 033015 (2023).

[48] P. Russer, Influence of microwave radiation on current-voltage characteristic of superconducting weak links, J. Appl. Phys. **43**, 2008 (1972).

[49] C. Ciaccia, R. Haller, A. C. C. Drachmann, T. Lindemann, M. J. Manfra, C. Schrade, and C. Schönenberger, Gate-tunable Josephson diode in proximitized InAs supercurrent interferometers, Phys. Rev. Res. **5**, 033131 (2023).

[50] A. Greco, Q. Pichard, and F. Giazotto, Josephson diode effect in monolithic dc-SQUIDs based on 3D Dayem nanobridges, Appl. Phys. Lett. **123**, 092601 (2023).

[51] C. Schrade, C. M. Marcus, and A. Gyenis, Protected hybrid superconducting qubit in an array of gate-tunable Josephson interferometers, PRX Quantum **3**, 030303 (2022).

[52] F. Lecocq, Dynamique quantique dans Un dcSQUID : Du Qubit de Phase à l'oscillateur Quantique Bidimensionnel, These de doctorat, Grenoble (2011).

[53] E. Dumur, A V-shape superconducting artificial atom for circuit quantum electrodynamics, These de doctorat, Université Grenoble Alpes (ComUE) (2015).

[54] C. W. J. Beenakker and H. Van Houten, Josephson current through a superconducting quantum point contact shorter

than the coherence length, Phys. Rev. Lett. **66**, 3056 (1991).

[55] D. C. Mattis and J. Bardeen, Theory of the anomalous skin effect in normal and superconducting metals, Phys. Rev. **111**, 412 (1958).

[56] M. Tinkham, *Introduction to Superconductivity*, 2nd ed., Dover Books on Physics (Dover., Mineola, 2015).

[57] D. S. Holmes and J. McHenry, Non-normal critical current distributions in Josephson junctions with aluminum oxide barriers, IEEE Trans. Appl. Supercond. **27**, 1 (2017).

[58] P. Dubos, H. Courtois, O. Buisson, and B. Pannetier, Coherent low-energy charge transport in a diffusive S-N-S junction, Phys. Rev. Lett. **87**, 206801 (2001).

[59] See Supplemental Material at http://link.aps.org/supplemental/10.1103/PhysRevResearch.6.033281 for additional information on devices characterization and measurements. It includes Refs. [52–58].